Journal of Molecular Catalysis B: Enzymatic 72 (2011) 298–304

Contents lists available at ScienceDirect

Journal of Molecular Catalysis B: Enzymatic

journal homepage: www.elsevier.com/locate/molcatb

ZnO nanoparticle and multiwalled carbon nanotubes for glucose oxidase direct electron transfer and electrocatalytic activity investigation

Fangxin Hu, Shihong Chen*, Chengyan Wang, Ruo Yuan*, Yaqin Chai, Yun Xiang, Cun Wang

Education Ministry Key Laboratory on Luminescence and Real-Time Analysis, College of Chemistry and Chemical Engineering, Southwest University, Chongqing 400715, China

ARTICLE INFO

Article history:
Received 31 March 2011
Received in revised form 5 July 2011
Accepted 5 July 2011
Available online 14 July 2011

Keywords:
Biosensor
Glucose oxidase
Direct electron transfer
ZnO nanoparticle
Multi-walled carbon nanotubes

ABSTRACT

A new amperometric enzyme biosensor for the determination of glucose has been constructed. Firstly, multiwalled carbon nanotubes (MWCNTs) were modified on the surface of a glassy carbon electrode (GCE). Then, the first layer of glucose oxidase (GOx) was assembled onto it. Subsequently, ZnO nanoparticles (nano-ZnO) were electrodeposited onto the electrode to immobilize the second layer of GOx. The assembly processes were characterized with cyclic voltammetry (CV), scanning electron microscopy (SEM) and atomic force microscopy (AFM). The direct electron transfer (DET) of immobilized GOx displays a pair of well defined and nearly reversible redox peaks with a formal potential ($E^{0'}$) of −0.434 V in pH 7.0 phosphate buffer solution. The electrochemical parameters including apparent heterogeneous electron transfer rate constant (k_s), charge transfer coefficient (α) and surface coverage (Γ) were estimated. The proposed enzyme biosensor showed a rapid and highly sensitive amperometric response to glucose in the range of 6.67 μM to 1.29 mM with a detection limit of 2.22 μM (S/N = 3). The apparent Michaelis–Menten constant (K_M^{app}) was calculated to be 2.48 mM. Furthermore, the biosensor showed an acceptable stability and reproducibility.

1. Introduction

Glucose is a keen metabolite for living organisms, especially in the case of patients suffering from diabetes [1]. The metabolic disorder results from insulin deficiency and hyperglycemia are reflected by blood glucose concentration higher or lower than the normal range of 4.4–6.6 mM [2]. As diabetes mellitus is a worldwide public health problem, an accurate measurement of glucose level in blood has long been recognized as an important clinical test for diagnosing diabetes mellitus [3]. Besides, an accurate measurement of glucose level is very important in a number of ways, like food industry for quality control purposes, fermentation, biological analysis and environmental monitoring [4,5]. Since the fabrication of the first glucose biosensor in 1962, various techniques such as fiber optic sensor [6], chemiluminescence [7] and fluorescence [8] have been reported. Compared to the methods mentioned above, electrochemical enzyme biosensor exhibits its own advantages, for example, simplicity, relatively low cost, high selectivity and sensitivity [9]. Virtues of the enzyme-based electrochemical biosensor gained itself extensive investigation.

Recently, there has been substantial attention in the direct electron transfer (DET) between redox proteins and electroactive biomolecules on the electrode surfaces. However, direct electrochemistry of most redox enzymes on bare solid electrodes is difficult to achieve because of the instability of the biological matrix upon interaction with the electrode surface and the deeply embedded active site in the proteins [10]. In order to overcome this drawback, current biosensors have turned to combine the properties of biologically active substances with nanomaterials. Nanomaterials provide high surface areas for enzyme loading and afford a favorable microenvironment which is propitious to help the enzyme to retain its bioactivity. In addition, the nanomaterials assist DET between enzyme's active site and electrode [11]. Therefore, variety of nanomaterial have been utilized to construct biosensors to promote DET, such as carbon nanotubes (CNTs) [12], colloidal gold nanoparticles [13], silver nanoparticle [14], mesoporous silica-SBA-15 [15], biomimetically synthesized silica [16], a-zirconium phosphate [17], porous nanosheet-based ZnO [18] and so on.

Nano-ZnO is a typical semiconductor material with a wide band gap (E_g = 3.37 eV) and a large exciton binding ability (60 meV) [19]. Due to its nontoxicity, biological compatibility, high catalytic efficiency, strong adsorption ability, fast electron transfer rate and easy preparation [19,20], nano-ZnO has been a favorable material for immobilization of biomolecule for developing biosensors. The high isoelectric point (IP: 9.5) of nano-ZnO makes it suitable for absorption of GOx with low IP of 4.2, as the protein immobilization is primarily driven by electrostatic

* Corresponding authors. Tel.: +86 23 68253172; fax: +86 23 68253172.
E-mail addresses: cshong@swu.edu.cn (S. Chen), yuanruo@swu.edu.cn (R. Yuan).

1381-1177/$ – see front matter © 2011 Elsevier B.V. All rights reserved.
doi:10.1016/j.molcatb.2011.07.005

interaction [21]. And nano-ZnO promotes the DET between the GOx and the electrode to a large extent. A tetragonal pyramid-shaped porous ZnO (TPSP-ZnO) nanostructure was used for the immobilization, direct electrochemistry and biosensing of proteins by Dai et al., which obtained a linear response to glucose concentrations ranging from 0.05 to 8.2 mM with a detection limit of 0.01 mM [2].

As is well known, CNTs have been extensively used in electrochemical studies and biosensor conformation [4]. Since discovery, CNTs have attracted considerable studies owing to their low electrical resistance, high accessible surface area, good mechanical strength, and excellent chemical stability [22]. Possessing many unique properties such as high electrocatalytic effect, strong adsorption ability, and excellent biocompatibility [23], CNTs are often used as reinforcing agents in composite coating [24]. Furthermore, CNTs behave good electronic communication with redox proteins even it is embedded deep with the glycoprotein sheath such as glucose oxidase (GOx) [4]. Silicon dioxide coated magnetic nanoparticle decorated multiwalled carbon nanotubes (Fe_3O_4@SiO_2/MWCNTs) were used to construct a new type of amperometric glucose biosensor [25]. Wang and co-workers prepared a carbon nanotube/chitosan/gold nanoparticles (CNT/CS/Au) based glucose biosensor with layer-by-layer technique [26].

Recently, the research interest has extended to modify CNTs with other nanomaterials such as semiconductor nanoparticles and metal nanoparticles since the composite materials possess properties of the individual components and simultaneously have outstanding synergistic effects [27]. Some investigations have been conducted for the fabrication of biosensors based on the nanocomposites consisted of CNTs and metal nanoparticles [28]. Also, nano-ZnO and MWCNTs composite is already used in constructing sensors. A hydroxylamine electrochemical sensor based on electrodeposition of porous ZnO nanofilms onto CNTs film has been fabricated [29]. Gold nanoparticles deposited on ZnO-MWCNTs film was used to analytical hydrazine [20]. Electrodeposition of zinc oxide (ZnO) nanoflowers onto CNTs film also performed well in detecting hydrogen peroxide [30]. Zhang et al. fabricated an electrochemical DNA biosensor based on ZnO/MWCNTs/chitosan nanocomposite, which was prepared by dispersing nano-ZnO and MWCNTs in chitosan (CS) solution. The remarkable synergistic effects of nano-ZnO and MWCNTs resulted in an improvement in the detection sensitivity for DNA hybridization [27].

In our previous work, we proposed an amperometric H_2O_2 biosensor based on the immobilization of Hemoglobin on the nanocomposite of MWCNTs and gold colloidal nanoparticles (GNPs) [28]. In this strategy, electrodepositing method and layer self-assembly technique were employed to fabricate glucose biosensor based on MWCNTs and nano-ZnO nanocomposite. Firstly, MWCNTs was modified on the surface of GCE to achieve the immobilization of the first layer of glucose oxidase (GOx). Subsequently, nano-ZnO was electrodeposited onto it to immobilize the second layer of GOx. This allowed us to take full advantage of the properties of MWCNTs, which not only helping to stabilize and fix the nano-ZnO onto the electrode surface but also to ensure extremely large surface area for the GOx loading quantity and fast mass transport. DET and electrocatalytic activity of GOx were investigated by cyclic voltammetry and amperometry techniques. The surface coverage (Γ), the value of formal potential ($E^{0'}$), charge transfer coefficient (α) and apparent heterogeneous electron transfer rate constant (k_s) of GOx were estimated. The integration of nano-ZnO and MWCNTs would offer potential promise for the fabrication of biosensors.

2. Experimental

2.1. Reagents and chemicals

MWCNTs (>95% purity) were purchased from Chengdu Organic Chemicals Co. Ltd. and purified by fluxing in concentrated nitric acid for 7 h prior to use. Glucose, glucose oxidase (E.C. 1.1.3.4, 151,000 U g^{-1}), chitosan (Mw: 100,000–300,000, deacetylating grade: 70–85%, from crab shells), were all purchased from Sigma. Potassium chloride and zinc nitrate were purchased from Chemical Reagent Company. All the other chemicals employed were analytical grade and were used as received. Phosphate buffer solutions (PBS) at various pH were prepared using 0.1 M Na_2HPO_4, 0.1 M KH_2PO_4, and 0.1 M KCl. Double-distilled water was used throughout the experiments. Glucose stock solution was kept at least 24 h after preparation for mutarotation. GOx solution was prepared with PBS and stored at 4 °C when not in use.

2.2. Apparatus

The electrochemical measurements were performed on a CHI660A electro-chemical work station (Shanghai, China). The conventional three-electrode system included a modified electrode as working electrode, a saturated calomel as reference electrode (SCE), and a platinum wire as auxiliary electrode. Scanning electron micrographs were studied with a scanning electron microscope (SEM, Hitachi, Japan). Atomic force microscopy (AFM) images were taken using scanning probe microscope (Vecco, USA).

2.3. Fabrication of the modified electrode

Glass carbon electrode (GCE) was polished carefully with 0.3 and 0.05 μm alumina on polishing cloth to obtain mirror like surface. Then it was rinsed with distilled water and followed by successive ultrasonic bath to remove the physically adsorbed substance.

MWCNTs were dispersed in 0.2-wt% chitosan (CS) solutions by using ultrasonic to obtain a CS-MWCNTs suspension (2.0 mg mL^{-1}) [30]. Then, the suspension was dropped onto the GCE surface and dried in room temperature to obtain the MWCNTs modified GCE. Subsequently, 5 μL GOx (2 mg mL^{-1}) was dropped onto MWCNTs/GCE and left for 12 h at 4 °C. With the GOx/MWCNTs/GCE used as the working electrode, electrodeposition of the nano-ZnO was performed in electrolytic solution containing 0.1 M KCl and 0.05 M $Zn(NO_3)_2$ at −1.2 V, room temperature for 20 min [29]. At the end of the growth duration, the substrate was removed from the solution and immediately rinsed in flowing deionized water to eliminate any residual salt from the surface and dried at room temperature, thus, the ZnO/GOx/MWCNTs/GCE was obtained. At last, 5 μL GOx (2 mg mL^{-1}) was dropped onto it and dried 12 h at 4 °C to obtain the GOx/ZnO/GOx/MWCNTs/GCE. The preparation process of the modified electrode is shown in Scheme 1. When not in use, the electrode was stored at 4 °C in a refrigerator.

3. Results and discussion

3.1. SEM and AFM characteristics of the modified films

The morphology of each modified film has been investigated by SEM. The SEM images were shown in Fig. 1. MWCNTs well dispersed in CS solution can be observed in Fig. 1a. Tubiform lines twisted and wrapped show themselves in the picture. After the enzyme loading, tubular structure of MWCNTs at the SEM image of GOx/MWCNTs film became relatively blurry in Fig. 1b. Fig. 1c shows particle-like morphology. This proves that nano-ZnO has been electrodeposited on the GOx/MWCNTs film successfully, and the nanoparticle diameter varies from 50 to 200 nm. After the second layer of GOx was

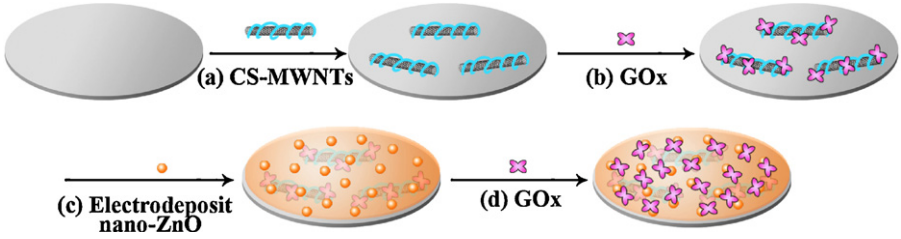

Scheme 1. Illustration of the preparation process of glucose biosensor.

dropped on the ZnO/GOx/MWCNTs film, a phenomenon can be observed in Fig. 1d that the dense clusters of GOx protein molecules were scattered on the whole surface of ZnO/GOx/MWCNTs film.

In order to further confirm the surface topographies of different films, AFM analysis were performed at MWCNTs film, GOx/MWCNTs film, ZnO/GOx/MWCNTs film and GOx/ZnO/GOx/MWCNTs film. Tubular structures can be found in Fig. 2a, which indicates the existence of MWCNTs. Its root mean square (RMS) roughness is 80.583 nm. After GOx was dropped on the MWCNTs as shown in Fig. 2b, a smoother configuration was presented with its RMS of 38.862 nm. When the electrodeposition was finished, sphere-like or particles-like nanostructures presented themselves in Fig. 2c, indicating that nano-ZnO was obtained. The RMS of this film increased to 59.820 nm correspondingly. In Fig. 2d, sphere-like or particles-like nanostructures became mistiness and the surface morphology became smoother (RMS was 22.336 nm), which might be ascribed to GOx filling the interstitial places between nano-ZnO and nano-ZnO, and between nano-ZnO and MWCNTs, suggesting that the GOx was effectively immobilized on the surface of ZnO/GOx/MWCNTs film.

3.2. Electrochemical characteristics and direct electron transfer of the modified electrode

The cyclic voltammograms (CVs) of different modified electrodes in 0.1 M PBS (pH 7.0) were investigated. As shown in Fig. 3, no obvious redox peaks appeared at MWCNTs/GCE (curve a). After immobilizing GOx, a pair of stable, well-defined and quasi-reversible redox peaks was observed which accorded with FAD to $FADH_2$ conversion (curve b). The peak current was decreased after electrodeposition of nano-ZnO (curve c) compared to GOx/MWCNTs, this might owing to the part filling of the electron transfer channel between enzyme and electrode by nano-ZnO. However, the peak current was greatly increased when the second layer of GOx was assembled onto the nano-ZnO modified electrode (curve d). On one hand, it was obvious that the double-layer enzyme structure increased the GOx loading amount significantly. On the other hand, the remarkable synergistic effects of nano-ZnO and MWCNTs promoted the DET of GOx greatly. Calculated from the average value of anodic and cathodic peak potentials, the formal potential ($E^{0'}$) of the FAD/$FADH_2$ redox couple was −0.434 V for the

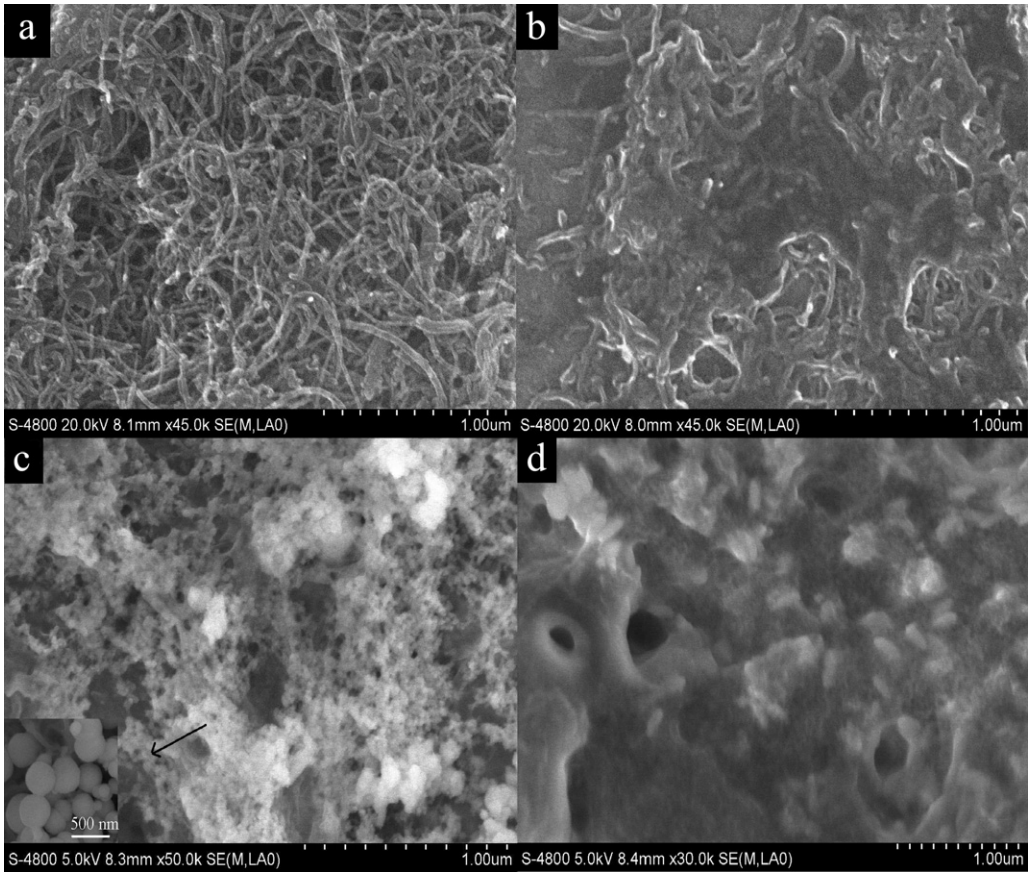

Fig. 1. SEM images of MWCNTs (a), GOx/MWCNTs (b), ZnO/GOx/MWCNTs at lower (c) and higher (inset in c) magnification and GOx/ZnO/GOx/MWCNTs modified film (d).

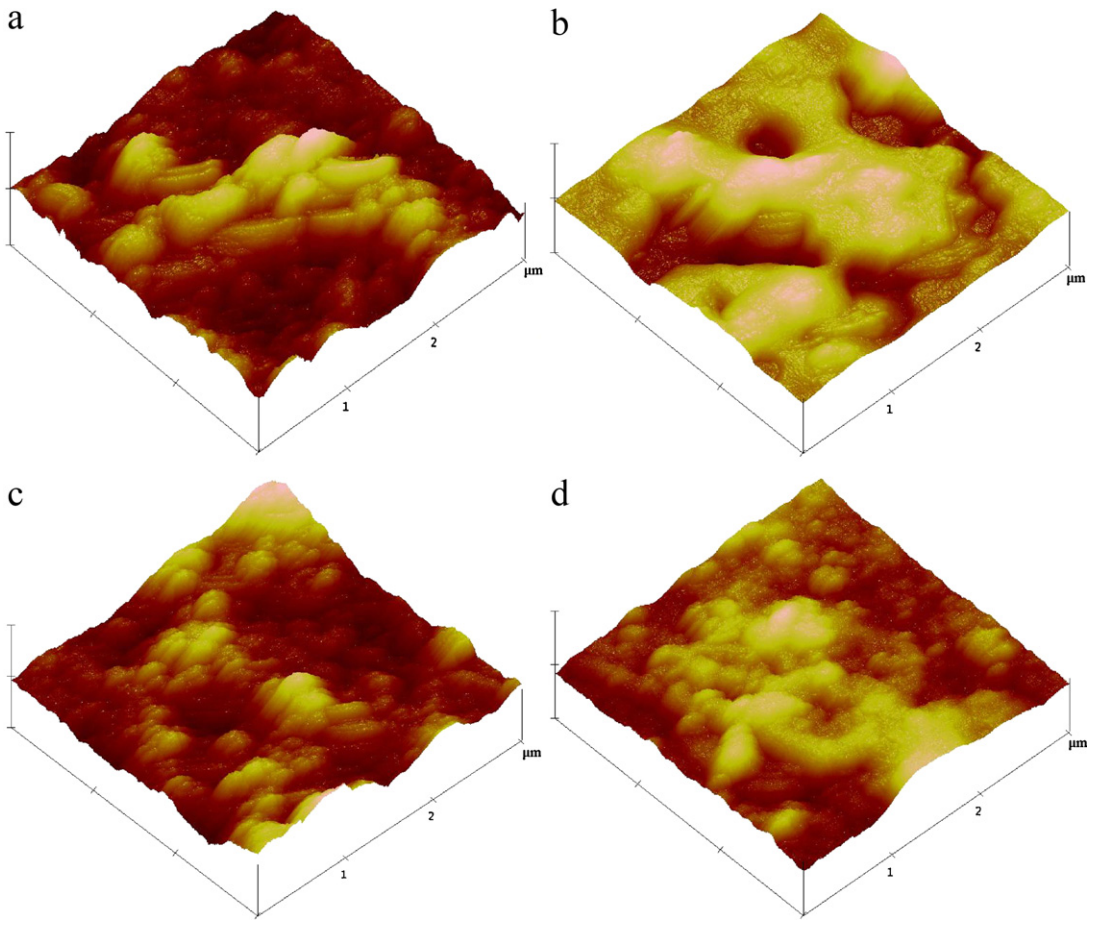

Fig. 2. AFM images of (a) MWCNTs, (b) GOx/MWCNTs, (c) ZnO/GOx/MWCNTs and (d) GOx/ZnO/GOx/MWCNTs modified film.

GOx/ZnO/GOx/MWCNTs film modified electrode. This value is very close to the FAD/$FADH_2$ standard potential, which is −0.460 V in pH 7.0 at 25.8 °C [31]. It confirms that the redox peak pairs which appear at the modified GCE are corresponding to the real direct redox behavior of the enzyme redox center (FAD). And the separation of anodic to cathodic peak potentials (ΔE_p) is 50 mV and ratio of anodic to cathodic peak current is about one.

To evaluate the reversible electron transfer phenomenon in more detail, the CVs at different scan rates were recorded in 0.1 M PBS (pH 7.0). As shown in Fig. 4A, both the anodic and the cathodic peaks currents are linearly proportional to the scan rate in the range of 10–600 mV s^{-1}, indicating a surface controlled electrochemical-oxidation/reduction of the FAD/$FADH_2$ involved in the GOx-structure. The surface coverage (Γ) of the electroactive GOx was investigated based on the following equation (Laviron) [32]:

$$Q = nFA\Gamma$$

where F is the Faraday constant, Q is the total amount of charge, n and A stand for electron transfer number and the electroactive surface area of the electrode, respectively. At first, the total amount of charge (Q) passed through the electrode for reduction or oxidation of electroactive species can be calculated through integration of CV peak [33]. Then, according to the relation between anodic peak current and square root of scan rate with the $[Fe(CN)_6]^{3-}/[Fe(CN)_6]^{4-}$ (5 mM) as probe, the electroactive surface area of electrode (A) was obtained as 0.3057 cm^2 with the equation [5]:

$$I_P = 2.69 \times 10^5 \times (D_0) \cdot C_0 \cdot A \cdot v^{1/2} \cdot n^{3/2}$$

Finally, the value of Γ was estimated to be 6.49×10^{-10} mol cm^{-2}, which is higher than the theoretical value (2.86×10^{-12} mol cm^{-2}) for the GOx monolayer deposited on the bare-electrode [31], suggesting that the nano-ZnO and MWCNTs provide a large and effective surface-area for enzyme immobilization. Meanwhile, it is larger than that was reported of 8.50×10^{-11} mol cm^{-2} for GOx immobilized on the poly-1,10-phenanthroline modified GCE (PPMH-GCE) [31].

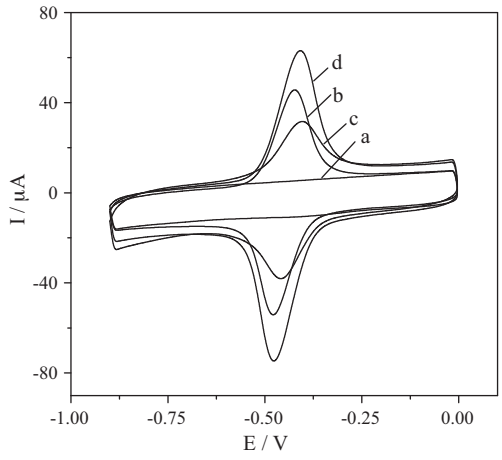

Fig. 3. CVs of the MWCNTs/GCE (a), GOx/MWCNTs/GCE (b), ZnO/GOx/MWCNTs/GCE (c), GOx/ZnO/GOx/MWCNTs/GCE (d) in 0.1 M PBS (pH 7.0) at a scan rate of 50 mV s^{-1}.

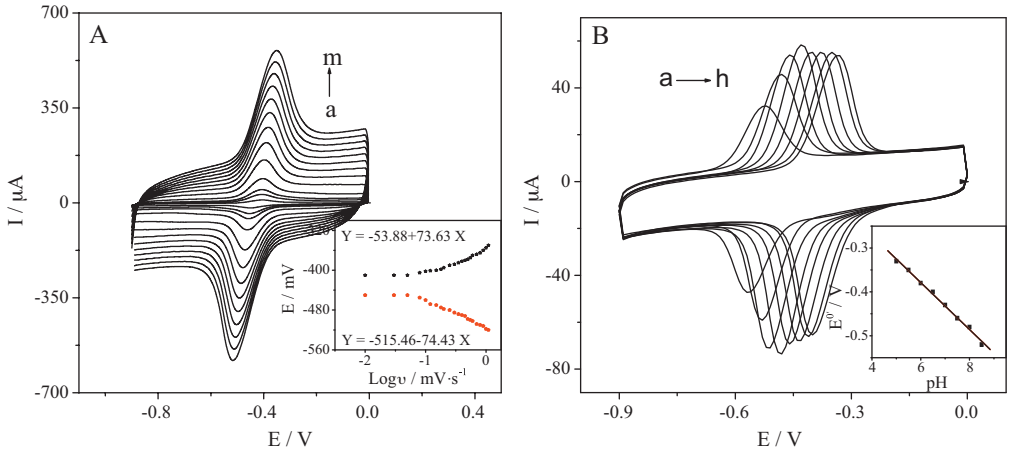

Fig. 4. (A) CVs of GOx/ZnO/GOx/MWCNTs/GCE at various scan rates in pH 7.0 PBS, from a to m, 10, 30, 50, 100, 200, 300, 400, 500, 600, 700, 800, 900 and 1000 mV s^{-1}. Inset: Anodic and cathodic peak potentials versus log (scan rates), respectively. (B) CVs of GOx/ZnO/GOx/MWCNTs/GCE at scan rate 50 mV s^{-1}, in different pH solutions (from a to h): 8.5, 8.0, 7.5, 7.0, 6.5, 6.0, 5.5 and 5.0. Inset: the plot of the formal potentials versus pH values.

The inset of Fig. 4A presents the Laviron plot of the dependency of peak potentials on logarithm (log) of scan rate for CVs. It can be seen from the plot that the peak potentials are independent on the relatively low scan rates, whereas, for scan rates above 200 mV s^{-1}, the peak potentials are proportional to the log (scan rates) as predicted by Laviron's theory [31]. The charge transfer coefficient (α) is calculated as 0.397, according to the formula:

$$E_{pc} = E^{0'} - \frac{2.3RT}{\alpha nF}\mathrm{Log}\frac{\alpha}{RTK} \times nF\upsilon = E^{0'} - \frac{2.3RT}{\alpha nF}\mathrm{Log}\frac{nF\alpha}{RTK} - \frac{2.3RT}{\alpha nF}\mathrm{Log}\,\upsilon$$

Here, R is an ideal gas constant, T is the temperature in Kelvin degree, E_{pc} is the peak potential of cathode, $E^{0'}$ is the condition potential, υ is scan rate, F is Faraday constant.

The apparent heterogeneous electron transfer rate constant (k_s) can be calculated according to the model of Laviron for a surface-controlled electrode process. The equation is as follows [34]:

$$\mathrm{Log}\,k_s = \alpha\,\mathrm{Log}(1-\alpha) + (1-\alpha)\mathrm{Log}\,\alpha - \mathrm{Log}\frac{RT}{nF\upsilon} - \frac{\alpha(1-\alpha)nF\cdot\Delta E_p}{2.3RT}$$

where R is an ideal gas constant, T is the temperature in Kelvin degree, F is Faraday constant, υ is the scan rate and ΔE_p is the separation of anodic to cathodic peak potentials. When υ is taken as 200 mV s^{-1}, ΔE_p is calculated to be 70 mV, k_s is determined as 1.98 s^{-1}. The relatively higher value of k_s indicating the direct electron transfer between the GOx and the electrode was greatly facilitated. And this value is higher than that was reported for GOx promoted by CNTs (1.53 s^{-1}) [35] and GOx on the PPMH-GCE (1.32 s^{-1}) [31].

3.3. Effect of pH on the formal potential ($E^{0'}$) of GOx/ZnO/GOx/MWCNTs/GCE

Influence of pH to the formal potential ($E^{0'}$) of modified electrode was investigated, which was shown in Fig. 4B. For a series of the values of pH, from 5.0 to 8.5, a pair of stable and well-defined redox-peaks that belong to the FAD/$FADH_2$ forms was observed, which was bound to the enzyme molecule. FAD/$FADH_2$ is known to undergo a two-electron coupled with two-proton redox reaction. Both reduction and oxidation peak potentials of the FAD/$FADH_2$ redox couple of modified electrode were negatively shifted by increasing the value of pH. This response is due to the electron transfer from FAD to the reduced $FADH_2$ which is depicted as follows:

$$\mathrm{FAD} + 2e^- + 2H^+ \rightarrow \mathrm{FADH_2}$$

As shown in the inset of Fig. 4B, the relation between the values of pH and the formal potentials ($E^{0'}$) can be expressed as:

$$E^{0'} = -53.57\mathrm{pH} - 57.14 (R = 0.9975)$$

The slope for a linear plot of $E^{0'}$ versus pH is −53.57 mV pH^{-1}, which is close to the theoretical one (−58.6 mV pH^{-1}) at 25 °C for a reversible, two-proton couple with two-electron redox reaction process [35,36]. Thus the formal potential ($E^{0'}$) of GOx immobilized on the surface of nano-ZnO and MWCNTs should be pH dependent.

3.4. Optimization of experimental parameters

The optimum pH for modified electrode was selected by amperometric response in a series of PBS from 5.0 to 8.5, containing 0.3 mM glucose. The amperometric currents achieved the highest value at pH 7.0, which indicates that pH 7.0 was optimum (see Supplementary Material Fig. S1A).

The effect of applied potential on response of the GOx/ZnO/GOx/MWCNTs/GCE towards glucose was also investigated through amperometric response of the biosensor to 0.3 mM glucose on the applied potential in the range from 0 to −0.60 V (see Supplementary Material Fig. S1B). The amperometric current gradually increasing with the applied potential varies from 0 to −0.60 V. And the current has a sharp increase at −0.30 V. Considering the interference of many coexisted foreign species at too negative potential, −0.30 V was chosen as the working potential to maintain a high sensitivity.

3.5. Amperometric response of the glucose biosensor

The amperometric current–time curve of GOx/ZnO/GOx/MWCNTs/GCE upon successive addition glucose to a continuous stirred PBS (pH 7.0) was recorded in curve a (Fig. 5A) under the optimized conditions. This biosensor exhibited a rapid response for the addition of glucose, and achieved 95% of the steady-state current within 10 s. Curve a (Fig. 5B) pictured the calibration curve of the GOx/ZnO/GOx/MWCNTs/GCE for glucose determination and its equation was $I(\mu A) = -4.66 + 3.02C_{\mathrm{glucose}}(\mathrm{mM})$ with a correlation coefficient of 0.9981. A good linear relationship was found between the chronoamperometric current and glucose concentration from 6.67 μM to 1.29 mM, meanwhile the detection limit of 2.22 μM was estimated at signal-to-noise ration of 3. The reached sensitivity was 10.03 μA mM^{-1} cm^{-2}, which is higher than reported glucose

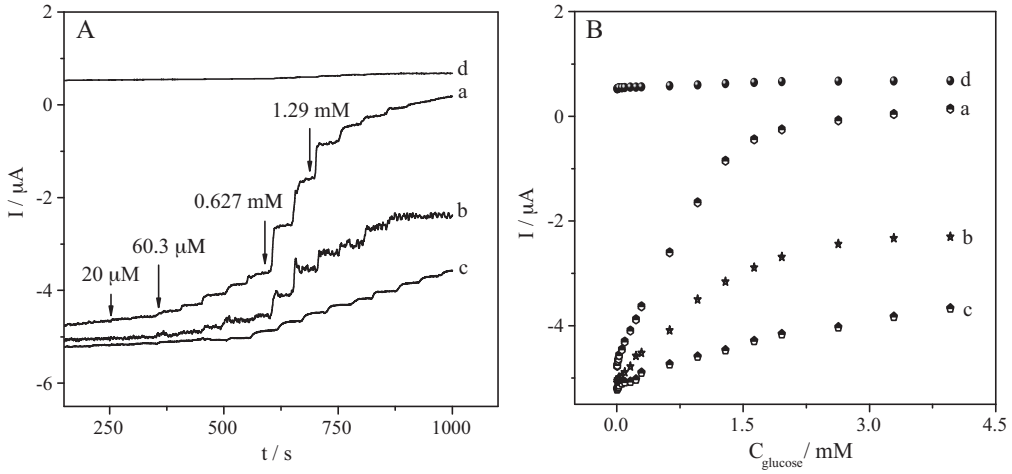

Fig. 5. (A) Current–time curves of the GOx/ZnO/GOx/MWCNTs/GCE (a), GOx/ZnO-MWCNTs/GCE (b), GOx/MWCNTs/GCE (c) and GOx/ZnO/GCE (d) at an applied potential of −0.30 V in 0.1 M pH 7.0 PBS. (B) The relation between concentrations of glucose and response currents for GOx/ZnO/GOx/MWCNTs/GCE (a), GOx/ZnO-MWCNTs/GCE (b), GOx/MWCNTs/GCE (c) and GOx/ZnO/GCE (d).

biosensor based on the electrodeposition of polypyrrole-MWCNTs-GOx nanobiocomposite film [37]. As presented in curve a (Fig. 5B), when the concentration of glucose was higher than 1.29 mM, the response of the GOx/ZnO/GOx/MWCNTs/GCE deviated from the straight line, showing the characteristics of Michaelis–Menten kinetics. The apparent Michaelis–Menten constant (K_M^{app}), a reflection of the enzymatic affinity, was calculated to be 2.48 mM according to the Lineweaver–Burk equation [38]:

$$\frac{1}{I_{ss}} = \frac{1}{I_{max}} + \frac{K_M^{app}}{I_{max}}\frac{1}{C}$$

Here, I_{ss} is the steady-state current after the addition of substrate, c is the bulk concentration of substrate and I_{max} is the maximum current measured under saturated substrate solution. The low value of K_M^{app} means that GOx immobilized on the nano-ZnO and MWCNTs composites retains well bioactivity and has a high affinity of the GOx to glucose.

As control experiments, the amperometric responses were also measured at GOx/ZnO-MWCNTs/GCE, GOx/MWCNTs/GCE and GOx/ZnO/GCE as shown in curve b, c and d (Fig. 5A), respectively. Their linear relationships were presented in Fig. 5B, correspondingly. As observed, both GOx/MWCNTs/GCE (curve c) and GOx/ZnO-MWCNTs/GCE (curve b) exhibited better response to glucose than GOx/ZnO/GCE (curve d), this sufficiently reveals the function of the MWCNTs in the construction of the biosensor. Compared to the GOx/ZnO-MWCNTs/GCE, GOx/MWCNTs/GCE and GOx/ZnO/GCE, the GOx/ZnO/GOx/MWCNTs/GCE achieved the highest response sensitivity towards glucose (Fig. 5A curve a), indicating that the double-layer enzyme structure is superior to the single layer structure with MWCNTs or nano-ZnO or ZnO-MWCNTs composite as immobilization matrix. This may be ascribed to the higher GOx loading amount of the double-layer enzyme structure and the remarkable synergistic effects of nano-ZnO and MWCNTs, which improved the detection sensitivity for glucose.

3.6. Stability, repeatability and interference determination

The storage stability of the proposed biosensor was studied. When not in use, the electrode was suspended above 0.1 M PBS at 4 °C in a refrigerator. The response of the biosensor to 0.6 mM glucose was tested intermittently. The biosensor lost about 6.4% and 14.9% of its original response after 10 days and 27 days, respectively. The biosensor also shows good reproducibility for the determination of glucose concentration in its linear range. The relative standard deviation (RSD) is 2.3% for five successive assays at the glucose concentration of 0.6 mM. This can be due to the good biocompatibility of MWCNTs and nano-ZnO, which provide a favorable microenvironment for GOx.

The selectivity and anti-interference ability of the biosensor were investigated by analyzing a standard solution of 0.6 mM glucose in existence of interfering species. 1.0 mM L-cysteine, 1.0 mM glycin, 1.0 mM ascorbic acid and 1.0 mM dopamine did not cause any observable interference to the response of glucose (see Supplementary Material Fig. S2). Thus, the proposed biosensor showed a high selectivity and good anti-interference ability.

3.7. Comparison of the performance at different modified electrodes

3.7.1. Comparison of the surface coverage and electron transfer rate constant

In order to further clarify the advantage of the GOx/ZnO/GOx/MWCNTs/GCE with double-layer enzyme structure, the Laviron plot of the relationship between peak potentials and log (scan rate) were also detected at GOx/ZnO-MWCNTs/GCE and GOx/MWCNTs/GCE (see Supplementary Material Fig. S3). And the value of Γ as well as k_s was investigated in details. As observed in Table 1, the proposed biosensor (GOx/ZnO/GOx/MWCNTs/GCE) held the highest value of Γ and k_s, indicating that the double-layer enzyme structure endowed the modified electrode higher amounts of bound enzyme than the single layer enzyme structure and the remarkable synergistic effects of nano-ZnO and MWCNTs greatly facilitated the electron-transfer between the GOx and the electrode.

3.7.2. Comparison with other glucose biosensors based on nano-ZnO

As depicted by Zhao et al. [39] and Rahman et al. [40], ZnO nanomaterials have been broadly applied to construct glucose biosensors. A comparison has been done between previous works

Table 1
Comparison of the surface coverage and electron transfer rate constant.

Different modified electrodes	Surface coverage (Γ/mol cm^{-2})	Electron transfer rate constant (k_s/s^{-1})
GOx/MWCNTs/GCE	3.12×10^{-10}	0.58
GOx/ZnO-MWCNTs/GCE	4.36×10^{-10}	0.98
GOx/ZnO/GOx/MWCNTs/GCE	6.49×10^{-10}	1.98

Table 2
Comparison of the performance of previous works and this work.

Structures of ZnO nanomaterials	Linear response range (mM)	Detection limit (μM)	K_M^{app} (mM)	Reference
TPSP-ZnO	0.05–8.2	10	/	[2]
ZnO nanoclusters	0–4	20	21	[41]
ZnO nanonails	0.1–7.1	5	15	[42]
ZnO nanorods	0.01–3.45	10	2.9	[43]
ZnO nanorods	0.005–0.3	3	/	[44]
ZnO nanoparticles	0.0067–1.29	3.33	2.48	This work

and this work. As shown in Table 2, our biosensor based on nano-ZnO and MWCNTs composites possesses the lower K_M^{app}, wider linear range and lower detection limit, suggesting the proposed biosensor has its advantages compared with other biosensor.

4. Conclusion

In this paper, the nanocomposite of MWCNTs and nano-ZnO was developed for the fabrication of an amperometric enzyme biosensor for the determination of glucose. Electrodepositing method and layer self-assembly technique were adopted to achieve the immobilization of two layers of GOx on the electrode. The integration of nano-ZnO and MWCNTs with its large surface area and good charge-transport characteristics increased the GOx loading amount and improved the detection sensitivity for glucose as compared to GOx/ZnO-MWCNTs/GCE, GOx/MWCNTs/GCE and GOx/ZnO/GCE. The remarkable synergistic effects of nano-ZnO and MWCNTs would offer potential promise for the fabrication of biosensors.

Acknowledgements

This work was supported by the National Natural Science Foundation of China (20675064), Key Lab of Chongqing Modern Analytical Chemistry, the Doctor Foundation of Southwest University (SWUB2008048) and the Fundamental Research Funds for the Central Universities (XDJK2009B013 and XDJK2009C082).

Appendix A. Supplementary data

Supplementary data associated with this article can be found, in the online version, at doi:10.1016/j.molcatb.2011.07.005.

References

[1] Y.Y. Wei, Y. Li, X.Q. Liu, Y.Z. Xian, G.Y. Shi, L.T. Jin, Biosens. Bioelectron. 26 (2010) 275–278.
[2] Z.H. Dai, G.J. Shao, J.M. Hong, J.C. Bao, J. Shen, Biosens. Bioelectron. 24 (2009) 1286–1291.
[3] M. Tasviria, H. Rafiee-Pourb, H. Ghourchianb, M.R. Gholami, J. Mol. Catal. B-Enzym. 68 (2011) 206–210.
[4] M.M. Rahman, A. Umarb, K. Sawada, Sens. Actuators B 137 (2009) 327–333.
[5] Z. Yang, Z.Z. Ye, B.H. Zhao, X.L. Zong, P. Wang, Physica E 42 (2010) 1830–1833.
[6] Z. Rosenzweig, R. Kopelman, Sens. Actuators B 35–36 (1996) 475–483.
[7] C.Y. Yang, Z.J. Zhang, Z.L. Shi, P. Xue, P.P. Chang, R.F. Yan, Talanta 82 (2010) 319–324.
[8] M. Lepore, M. Portaccio, E. De Tommasi, P. De Luca, U. Bencivenga, P. Maiuri, D.G. Mita, J. Mol. Catal. B-Enzym. 31 (2004) 151–158.
[9] L.P. Ma, R. Yuan, Y.Q. Chai, S.H. Chen, J. Mol. Catal. B-Enzym. 56 (2009) 215–220.
[10] M. Tasviri, H.A. Rafiee-Pour, H. Ghourchian, M.R. Gholami, J. Mol. Catal. B-Enzym. 68 (2011) 206–210.
[11] Y. Wang, R. Yuan, Y.Q. Chaia, W.J. Li, Y. Zhuo, Y.L. Yuan, J.J. Li, J. Mol. Catal. B-Enzym. 71 (2011) 146–151.
[12] Y. Liu, M.K. Wang, F. Zhao, Z.A. Xu, S.J. Dong, Biosens. Bioelectron. 21 (2005) 984–988.
[13] S. Zhao, K. Zhang, Y. Bai, W.W. Yang, C.Q. Sun, Bioelectrochemistry 69 (2006) 158–163.
[14] K. Murata, M. Suzuki, N. Nakamura, H. Ohno, Electrochem. Commun. 11 (2009) 1623–1626.
[15] K.Q. Wang, H. Yang, L. Zhu, J.H. Liao, T.H. Lu, W. Xing, S.Y. Xing, Q. Lv, J. Mol. Catal. B-Enzym. 58 (2009) 194–198.
[16] P. Zamora, A. Narváez, E. Domínguez, Bioelectrochemistry 76 (2009) 100–106.
[17] Y.G. Liu, C.L. Lu, W.H. Hou, J.J. Zhu, Anal. Biochem. 375 (2008) 27–34.
[18] X.B. Lu, H.J. Zhang, Y.W. Ni, Q. Zhang, J.P. Chen, Biosens. Bioelectron. 24 (2008) 93–98.
[19] X.L. Zhu, I. Yuri, X. Gan, I. Suzuki, G.X. Li, Biosens. Bioelectron. 22 (2007) 1600–1604.
[20] C.H. Zhang, G.F. Wang, Y.L. Ji, M. Liu, Y.H. Feng, Z.D. Zhang, B. Fang, Sens. Actuators B 150 (2010) 247–253.
[21] Y. Lei, X.Q. Yan, J. Zhao, X. Liu, Y. Song, N. Luo, Y. Zhang, Colloids Surf. B 82 (2011) 168–172.
[22] S.H. Lee, T.T.N. Doan, K. Won, S.H. Ha, Y. Koo, J. Mol. Catal. B-Enzym. 62 (2010) 169–172.
[23] S.L. Yang, X.Y. Liu, X.D. Zeng, B.Y. Xia, J.P. Gu, S.L. Luo, N.N. Mai, W.Z. Wei, Sens. Actuators B 145 (2010) 762–768.
[24] B.M. Praveen, T.V. Venkatesha, J. Alloys Compd. 482 (2009) 53–57.
[25] T.T. Baby, S. Ramaprabhu, Talanta 80 (2010) 2016–2022.
[26] Y. Wang, W.Z. Wei, X.Y. Liu, X.D. Zeng, Mater. Sci. Eng. C-Biomim. Supramol. Syst. 29 (2009) 50–54.
[27] W. Zhang, T. Yang, D.M. Huang, K. Jiao, G.C. Li, J. Membr. Sci. 325 (2008) 245–251.
[28] S.H. Chen, R. Yuan, Y.Q. Chai, L.Y. Zhang, N. Wang, X.L. Li, Biosens. Bioelectron. 22 (2007) 1268–1274.
[29] C.H. Zhang, G.F. Wang, M. Liu, Y.H. Feng, Z.D. Zhang, B. Fang, Electrochim. Acta 55 (2010) 2835–2840.
[30] H.P. Bai, X.X. Lu, G.M. Yang, Y.H. Yang, Chin. Chem. Lett. 19 (2008) 314–318.
[31] Y. Oztekin, A. Ramanaviciene, Z. Yazicigil, A.O. Solak, A. Ramanavicius, Biosens. Bioelectron. 26 (2011) 2541–2546.
[32] E. Laviron, J. Electroanal. Chem. 101 (1979) 19–28.
[33] Q.L. Wang, G.X. Lu, B.J. Yang, Biosens. Bioelectron. 19 (2001) 1269–1275.
[34] H.Y. Gu, A.M. Yu, H.Y. Chen, J. Electroanal. Chem. 516 (2001) 119–126.
[35] C.X. Cai, J. Chen, Anal. Biochem. 332 (2004) 75–83.
[36] A. Salimi, E. Sharifi, A. Noorbakhsh, S. Soltanian, Biosens. Bioelectron. 22 (2007) 3146–3153.
[37] Y.C. Tsai, S.C. Li, S.W. Liao, Biosens. Bioelectron. 22 (2006) 495–500.
[38] S.H. Chen, R. Yuan, Y.Q. Chai, B. Yin, W.J. Li, L.G. Min, Electrochim. Acta 54 (2009) 3039–3046.
[39] Z.W. Zhao, W. Lei, X.B. Zhang, B.P. Wang, H.L. Jiang, Sensors 10 (2010) 1216–1231.
[40] M.M. Rahman, A.J.S. Ahammad, J.H. Jin, S.J. Ahn, J.J. Lee, Sensors 10 (2010) 4855–4886.
[41] Z.W. Zhao, X.J. Chen, B.K. Tay, J.S. Chen, Z.J. Han, K.A. Khor, Biosens. Bioelectron. 23 (2007) 135–139.
[42] A. Umar, M.M. Rahman, S.H. Kim, Y.B. Hahn, J. Nanosci. Nanotechnol. 8 (2008) 3216–3221.
[43] A. Wei, X.W. Sun, J.X. Wang, Y. Lei, X.P. Cai, C.M. Li, Z.L. Dong, W. Huang, Appl. Phys. Lett. 89 (2006) 123902(1)–123902(3).
[44] X.W. Liu, Q.Y. Hu, Q. Wu, W. Zhang, Z. Fang, Q.B. Xie, Colloids Surf. B 74 (2009) 154–158.